BNL-222345-2021-JAAM

Redundant roles of four ZIP family members in zinc homeostasis and seed development in Arabidopsis thaliana

S. Lee, R. Tappero

To be published in "PLANT JOURNAL"

October 2021

Photon Sciences

Brookhaven National Laboratory

U.S. Department of Energy

USDOE Office of Science (SC), Basic Energy Sciences (BES) (SC-22)

DISCLAIMER

the plant journal

SEB SOCIETY FOR EXPERIMENTAL BIOLOGY

The Plant Journal (2021) doi: 10.1111/tpj.15506

Redundant roles of four ZIP family members in zinc homeostasis and seed development in *Arabidopsis thaliana*

Sichul Lee[1,2], Joohyun Lee[1,3], Felipe K. Ricachenevsky[1,4,5], Tracy Punshon[1], Ryan Tappero[6], David E. Salt[7] and Mary Lou Guerinot[1]*

[1]*Department of Biological Sciences, Dartmouth College, Hanover, NH 03755, USA,*
[2]*Center for Plant Aging Research, Institute for Basic Science (IBS), Daegu 42988, Korea,*
[3]*Division of Natural and Applied Sciences, Duke Kunshan University, Kunshan, Jiangsu 215306, China,*
[4]*Botany Department, Biosciences Institute, Federal University of Rio Grande do Sul, Porto Alegre, Brazil,*
[5]*Graduate Program in Cell and Molecular Biology, Biotechnology Center, Federal University of Rio Grande do Sul, Porto Alegre, Brazil,*
[6]*Brookhaven National Laboratory, Upton, NY 11973, USA, and*
[7]*Future Food Beacon of Excellence and the School of Biosciences, University of Nottingham, Loughborough LE12 5RD, UK*

Received 19 April 2021; revised 29 August 2021; accepted 8 September 2021.
*For correspondence (e-mail mary.lou.guerinot@dartmouth.edu).

SUMMARY

Zinc (Zn) is essential for normal plant growth and development. The Zn-regulated transporter, iron-regulated transporter (IRT)-like protein (ZIP) family members are involved in Zn transport and cellular Zn homeostasis throughout the domains of life. In this study, we have characterized four ZIP transporters from *Arabidopsis thaliana* (IRT3, ZIP4, ZIP6, and ZIP9) to better understand their functional roles. The four ZIP proteins can restore the growth defect of a yeast Zn uptake mutant and are upregulated under Zn deficiency. Single and double mutants show no phenotypes under Zn-sufficient or Zn-limited growth conditions. In contrast, triple and quadruple mutants show impaired growth irrespective of external Zn supply due to reduced Zn translocation from root to shoot. All four *ZIP* genes are highly expressed during seed development, and siliques from all single and higher-order mutants exhibited an increased number of abnormal seeds and decreased Zn levels in mature seeds relative to wild type. The seed phenotypes could be reversed by supplementing the soil with Zn. Our data demonstrate that IRT3, ZIP4, ZIP6, and ZIP9 function redundantly in maintaining Zn homeostasis and seed development in *A. thaliana*.

Keywords: ZIP transporter, *Arabidopsis thaliana*, zinc, seeds, high-order mutants, zinc homeostasis, abiotic stress.

INTRODUCTION

Zinc (Zn) is an essential element in all living organisms and acts as a structural or catalytic cofactor in a large number of enzymes and regulatory proteins, including RNA polymerase, superoxide dismutase, alcohol dehydrogenase, carbonic anhydrase, and the Zn finger family of transcription factors (Palmer and Guerinot, 2009; Sinclair and Krämer, 2012). Bioinformatic approaches estimate that the Zn-binding proteome ranges from 5 to 6% in prokaryotes and is about 10% in eukaryotes (Andreini et al., 2009).

Zn-deficient soils are widespread globally and Zn deficiency is estimated to affect about one-third of the world's human population who live on plant-based diets. Under Zn deficiency, plants have decreased growth, are more susceptible to stress, and have decreased chlorophyll synthesis, leading to a severe reduction in crop production (Sinclair and Krämer, 2012). The damage caused by Zn deficiency at the cellular level is presumably due to reactive oxygen species (Cakmak, 2000). Excess Zn can also cause serious harm, due to unregulated high-affinity binding to inappropriate intracellular ligands and uncontrolled displacement of essential cofactor metal cations (Palmgren et al., 2008). Therefore, plants must maintain physiologically adequate intracellular Zn levels using a tightly controlled metal homeostasis network capable of responding to fluctuations in Zn availability. This is largely achieved through Zn-dependent changes in the expression of genes involved in the uptake, transport, and storage of Zn (Lilay et al., 2021).

Zn transporters mediate the cellular influx and efflux of Zn. The Zn-regulated transporter/iron-regulated transporter (IRT)-like protein (ZIP) family members have been

reported to transport Zn as well as Fe and Mn into the cytoplasm from either outside of cells or intracellular organelles/vesicles (Hu, 2021). The ZIP family was first identified in *Arabidopsis thaliana* (Eide et al., 1996) and we now know that members of this family are found throughout all domains of life (Hu, 2021). Many members of the *A. thaliana ZIP* gene family have been shown to be expressed throughout the plant and are upregulated under Zn deficiency, and many can transport Zn when expressed in yeast (Grotz and Guerinot, 2006; Lin et al., 2009; Milner et al., 2013). However, up until now we did not have strong *in planta* experimental evidence as to which *A. thaliana* ZIP family members are important for Zn uptake from the soil and for maintaining Zn homeostasis. Overexpression of *IRT3* results in increased accumulation of Zn in the shoot and Fe in the root of transgenic lines, suggesting that IRT3 functions as a Zn and Fe uptake transporter in *A. thaliana*, but this study did not include characterization of an *irt3* mutant (Lin et al., 2009). A number of loss of function mutants (*zip1*, *zip2*, *zip5*, *zip6*, *zip9*, *zip12*) have been examined, including *Arabidopsis halleri zip6*, but none have a strong Zn-related phenotype (Inaba et al., 2015; Milner et al., 2013; Spielmann et al., 2020; Wu et al., 2009). This certainly suggests that many of the ZIP family members play redundant roles in Zn homeostasis. Indeed, recent work in rice (*Oryza sativa*) has shown that two tandem duplicated genes, *OsZIP5* and *OsZIP9*, function redundantly in Zn uptake (Tan et al., 2020). *OsZIP5* and *OsZIP9* are both expressed in the root epidermis and respond to the local Zn status in the root; *OsZIP9* is also regulated by systemic signals of Zn status from the shoot. *oszip9* mutants show impaired Zn uptake and growth retardation (Huang et al., 2020; Tan et al., 2020; Yang et al., 2020). *oszip5* mutants also show decreased Zn uptake, although their phenotype is less severe compared to that of the *oszip9* mutant (Tan et al., 2020). The double mutant *oszip5 oszip9* showed an enhanced Zn deficiency phenotype compared with the single mutants (Tan et al., 2020). These are the first Zn transporters unequivocally shown to be responsible for uptake from the soil and the first example of the functional overlap among ZIP family members (Tan et al., 2020).

In order to understand the role of the *A. thaliana* ZIP family members in Zn transport, we examined the function of four putative Zn transporters, IRT3, ZIP4, ZIP6, and ZIP9. We were particularly interested in the role of these transporters in seed development as previous loss of function studies in *A. thaliana* did not examine seed phenotypes. Zn plays a vital role in seed development with reproductive organs having a high requirement for Zn (Krämer and Clemens, 2005). Using single mutants for each gene, we generated double, triple, and quadruple knockout mutants to investigate their functional redundancy. Triple and quadruple mutants showed decreased growth irrespective of Zn supply due to reduced Zn translocation from root to shoot. Furthermore, all single and higher-order mutants exhibited abnormal seed development, with higher-order mutants having more severe defects, suggesting redundant roles for both vegetative growth and reproductive organ development.

RESULTS

Single and double mutants of *IRT3*, *ZIP4*, *ZIP6*, and *ZIP9* do not affect seedling growth or Zn distribution

In order to begin to understand the function of various understudied members of the ZIP family in Arabidopsis and to determine whether any of these members act redundantly, we decided to create higher-order mutants of three *ZIP* genes (*IRT3*, *ZIP4*, *ZIP9*) that encode proteins with high amino acid similarity and form a subgroup based on phylogenetic analysis (Evens et al., 2017). We also decided to investigate ZIP6, which does not cluster with any other ZIP family members (Evens et al., 2017) and, as such, might be expected to have a unique role in Zn homeostasis.

Functional complementation in yeast showed that all four ZIP proteins can transport Zn (Figure 1a) but not Fe or Mn (Figure S1). We note here that Milner et al. (2013) previously reported that ZIP6 and ZIP9 cannot transport Zn but can transport Mn, and Lin et al. (2009) reported that IRT3 could transport Fe as well as Zn. The differences may be explained by the use of different cDNA clones and expression systems. We confirmed that the expression of all four genes is induced in roots when plants are grown under Zn-deficient conditions (Figure 1b). Expression of *IRT3* and *ZIP6* was also increased in Zn-deficient shoots, whereas *ZIP4* and *ZIP9* expression levels were not affected. Under Fe-deficient growth conditions, expression of *ZIP9* was upregulated both in shoot and roots (Figure 1b). We also examined the temporal and spatial expression of the four *ZIP* genes, using transgenic plants harboring 1 kb of promoter sequence fused to a GUS-encoding reporter gene. When plants were grown under Zn-deficient growth conditions, expression in roots was enhanced in all transgenic plants (Figure 2a), consistent with our quantitative PCR (qPCR) analysis (Figure 1b). The GUS staining experiments indicated that the four *ZIP* genes were mainly expressed in the root stele when plants were grown under Zn limitation. In Zn-limited shoots, expression of *IRT3* and *ZIP6* was increased relative to Zn-sufficient conditions, whereas *ZIP4* and *ZIP9* expression was low regardless of growth conditions (Figure 2a), again in agreement with our qPCR data. In older leaves, we could detect GUS expression mainly in the vascular tissues for all *ZIP* proteins except ZIP9 (Figure 2b–d). During the reproductive stage, GUS expression driven by the *IRT3*, *ZIP4*, and *ZIP6* promoters was seen in the flowers and developing seeds (Figure 2b–d). Examination of publicly available expression

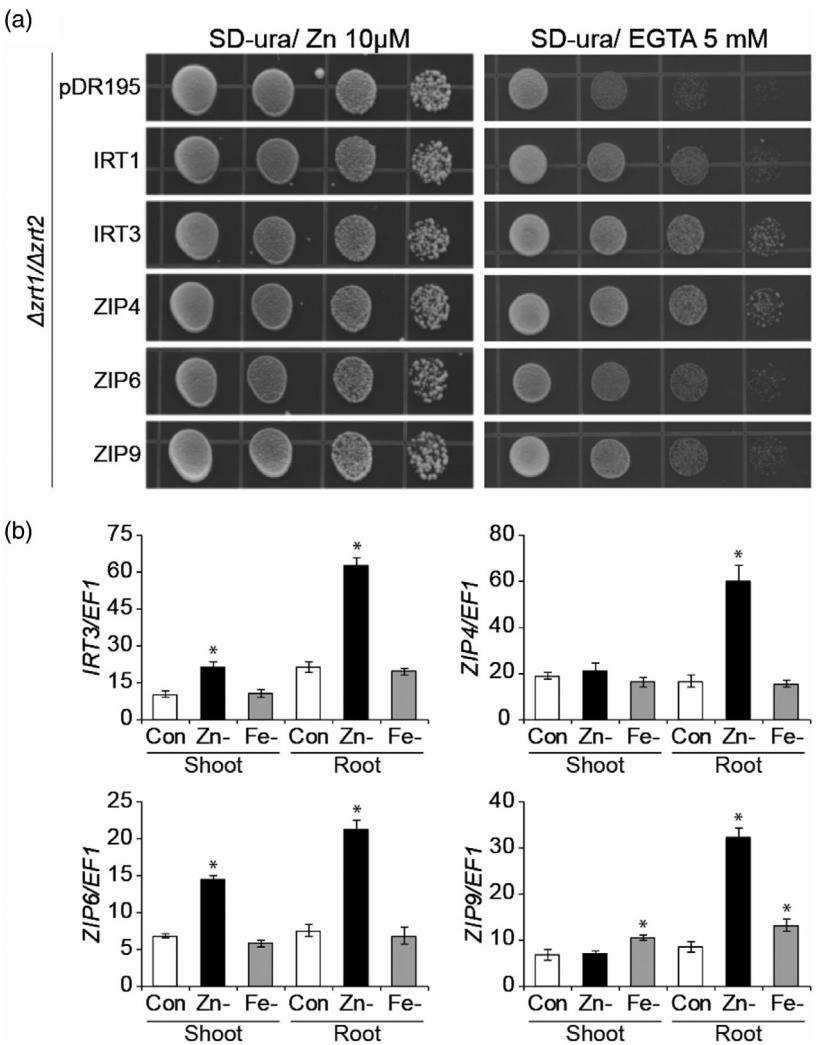

Figure 1. Functional complementation of a yeast Zn uptake mutant and expression analysis of *Arabidopsis thaliana ZIP* genes under micronutrient deficiencies. (a) Complementation test of the Zn uptake-defective yeast mutant *zrt1 zrt2*. Yeast cells were transformed with empty vector pDR195 or a construct containing a *ZIP* cDNA. IRT1 was used as a positive control. After growth overnight, the cell concentration was adjusted to OD_{600} = 1.0 and then serially diluted 10-, 100-, and 1000-fold. For the assay, 5 μl of each dilution was plated out onto control or Zn-limited medium and grown for 3 days at 30°C. (b) Quantitative real-time PCR analysis of four *ZIP* genes in shoots and roots of *A. thaliana* seedlings grown on control or Zn- or Fe-deficient medium. Expression is shown relative to *EF1α*. Error bars represent the standard error of three replicates. Asterisks above the bars indicate significant differences from the control growth condition by Student's *t*-test ($P < 0.05$).

profiles of *A. thaliana ZIP* genes revealed that *IRT3*, *ZIP4*, and *ZIP6* are all highly expressed during flower and seed development (Figure S2), in agreement with the results from the promoter-GUS lines.

To investigate the subcellular localization of the four ZIP proteins, we generated transgenic Arabidopsis plants expressing green fluorescent protein (GFP) translational fusions for the four ZIP proteins, driven by the CaMV *35S* promoter. Green fluorescence signals were detected in the plasma membrane (PM) (Figure S3), and propidium iodide (PI) was used to stain the PM. Co-localization of GFP and PI signals strongly suggests that the four ZIP proteins all localize to the PM. Taken together, our results suggest that these four ZIPs act as PM-localized Zn transporters.

In order to characterize the functional role of each *ZIP* gene in regulating Zn homeostasis, we isolated transfer DNA (T-DNA) mutants for each of the four *ZIP* genes (Figure S4a). The T-DNA insertion in *irt3-1* is located in the promoter (Figure S4a), leading to reduced expression relative to wild type (WT) when this mutant is grown under Zn-sufficient conditions and no induction of *IRT3* expression under Zn deficiency (Figure S4b). *zip4-2*, *zip4-3*, *zip6-1*, *zip6-2*, and *zip9* are loss of function mutants, with no expression detected (Figure S4c–e). When the T-DNA lines were grown on medium containing Zn, no obvious phenotypes were observed compared to WT (Figure S5a). Their fresh weight and root length were similar to those of WT (Figure S5b,c). Under Zn deficiency, the growth of the T-DNA mutants was similar to that of WT, as shown by the similar biomass and root length (Figure S5a–c). To determine whether disruption of any of the four *ZIP* genes affected Zn distribution, we measured the Zn concentrations in shoots and roots of plants grown under Zn-sufficient and Zn-deficient conditions. Compared with WT, the mutants accumulated similar levels of Zn in shoots and roots, reflecting the lack of phenotypic differences (Figure S5d,e).

We next generated double mutants and grew the plants under Zn-sufficient or Zn-deficient growth conditions. The

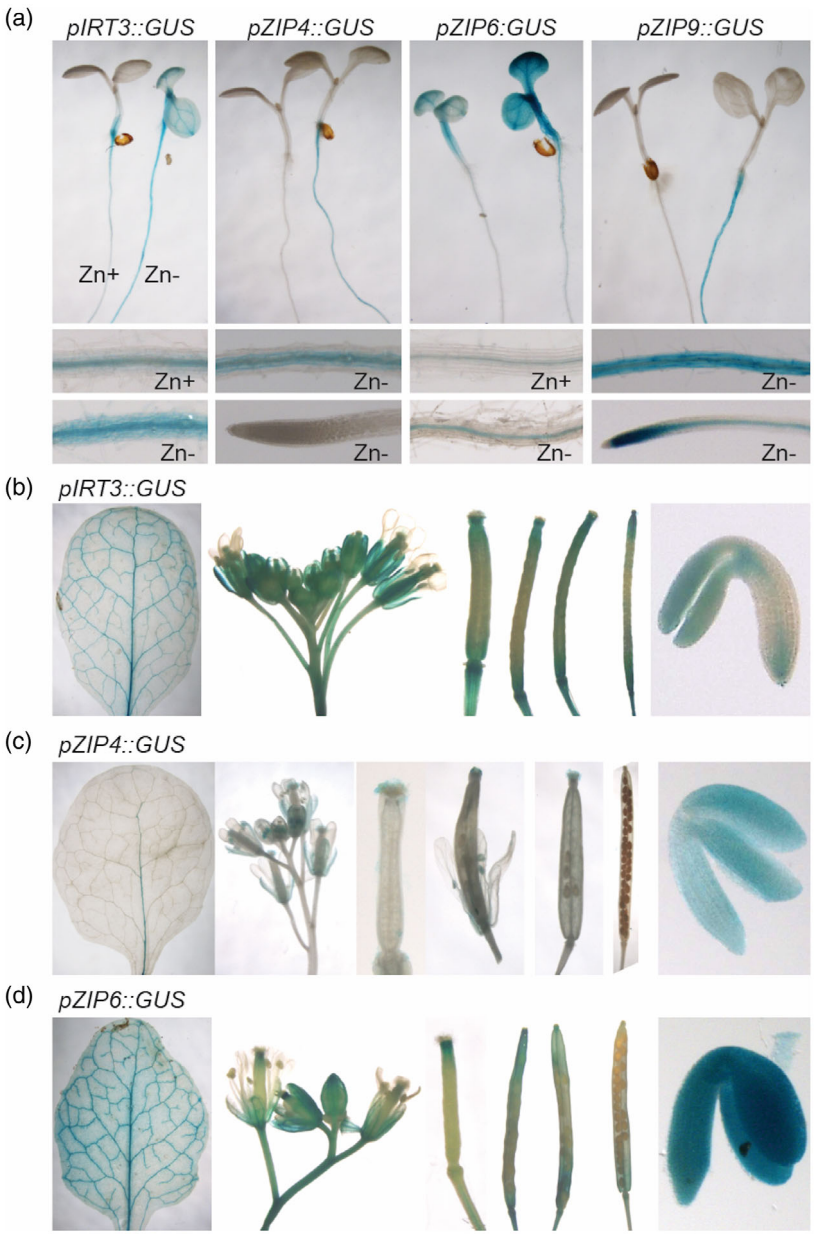

Figure 2. Spatial and temporal expression of *Arabidopsis thaliana ZIP* genes in promoter-GUS transgenic plants. (a) Four-day old seedlings grown under Zn deficiency (Zn−) or Zn sufficiency (Zn+). Whole seedlings are shown in the top row with sections of roots shown in the middle and bottom rows (a). (b–d) GUS expression patterns of 7-week-old leaves, flowers, siliques, and developing seeds from *pIRT3*::*GUS* (b), *pZIP4*::*GUS* (c), and *pZIP6*::*GUS* (d).

double mutants did not show any obvious morphological phenotypes as compared to WT, regardless of growth conditions (Figure S6a). Quantification of fresh weight and root length also indicated that there were no significant differences between WT and double mutants (Figure S6b,c). When we compared the Zn concentrations in shoots and roots, double mutants showed levels similar to those of WT (Figure S6d,e).

Quadruple and triple mutants have impaired seedling growth and altered Zn distribution

As single and double T-DNA mutants did not show any obvious phenotypes at the seedling stage, we generated triple and quadruple mutants. Two triple mutants (*tko-1*: *irt3-1/zip4-2/zip6-1* and *tko-2*: *irt3-1/zip4-2/zip9-1*) and one quadruple (*qko*: *irt3-1/zip4-2/zip6-1/zip9-1*) mutant were isolated. Quadruple and triple mutants were smaller than WT, irrespective of Zn supply (Figure 3a,b). Under Zn sufficiency, the fresh weights of *qko*, *tko-1*, and *tko-2* mutants were 76.6, 84.8, and 88.4% compared to WT, respectively; without Zn, fresh weights were 83.2, 87.9, and 88.5% compared to WT fresh weight, respectively (Figure 3c). Root lengths of *qko*, *tko-1*, and *tko-2* were 72.7, 82.8, and 86.7% compared to WT under Zn supply, and 65.8, 80.7, and 82.1% compared to WT under Zn deficiency relative to WT, respectively (Figure 3d).

To assess whether disruption of three or four *ZIP* genes affects Zn distribution, we measured the Zn concentrations in shoots and roots at the seedling stage grown on Zn-sufficient or Zn-limited media (Figure 3e,f). Zn concentrations in shoots from *qko*, *tko-1*, and *tko-2* were lower than that of WT, regardless of the Zn supply (Figure 3e,f). On the contrary, roots from quadruple and triple mutants accumulated more Zn as compared to WT (Figure 3e,f). Therefore, we observed that the shoot:root ratios of Zn concentrations of WT were higher than those of *qko*, *tko-1*, and *tko-2*, suggesting less efficient root-to-shoot translocation of Zn in mutants than in WT (Figure 3g). Because root Fe uptake can interact and interfere with Zn uptake (Milner et al., 2013), we assessed the effects of four ZIPs on the distribution of Fe at the seedling stage under Zn-sufficient or Zn-deficient growth conditions. The results indicated that there were no differences in Fe concentration among genotypes, and therefore the shoot:root ratios of Fe concentrations were not different (Figure S7).

Next, we examined whether the triple or quadruple mutants changed the distribution of Zn within the roots using Zinpyr-1 (Figure 3h–k). Zinpyr-1 is a Zn fluorophore that has been previously used to examine the localization of Zn in roots in *A. thaliana* (Sinclair et al., 2007). In WT, green fluorescence was abundant in the stele where the four *ZIP* genes are normally expressed (Figure 3h). By contrast, the strongest fluorescence signal was observed in the cortex and endodermis in the quadruple and triple mutants (Figure 3i–k).

Because quadruple and triple mutants modified Zn distribution and translocation between shoot and root, we monitored the sensitivity of seedlings to Zn toxicity. When quadruple and triple mutants were exposed to excess Zn at the seedling stage, they showed better growth and had longer roots than WT (Figure S8).

Altered expression of Zn homeostasis-related genes in seedlings of the quadruple and triple mutants

As quadruple and triple mutants exhibited defective seedling growth, we investigated the transcript levels of several genes related to Zn homeostasis in the WT and quadruple and triple mutants under Zn-sufficient or Zn-deficient growth conditions (Figure S8). First, we analyzed the expression of four *A. thaliana nicotianamine synthetase* (*NAS*) genes. NAS catalyzes the formation of nicotianamine (NA), which is involved in the long-distance distribution of metals in plants and is important for cellular metal homeostasis in all tissues (Schuler et al., 2012). In WT, expression of *NAS2*, *NAS3*, and *NAS4* was higher when plants were grown under Zn-deficient than under Zn-sufficient growth conditions, while *NAS1* was not changed by different external Zn supply (Figure S9a–d). In the quadruple and triple mutants, Zn deficiency enhanced the expression of *NAS1* and *NAS3* (Figure S9a,c), and transcript levels of *NAS2* were increased in shoot and root irrespective of Zn status (Figure S9b). The expression of *NAS4* was increased only in Zn-deficient shoots (Figure S9d).

Next, we analyzed the expression levels of *HMA2* and *HMA4*, which are located in the PM and involved in the long-distance translocation of Zn (Hussain et al., 2004). In the mutants, expression of *HMA2* was decreased in roots relative to WT regardless of Zn concentration (Figure S9a), and *HMA4* transcripts were decreased in both roots and shoots of mutants both under Zn-sufficient and Zn-deficient growth conditions (Figure S9f). We also analyzed the transcript levels of *MTP1* and *MTP3*, which are located at the vacuolar membrane and contribute to basal Zn tolerance (Arrivault et al., 2006; Kawachi et al., 2009; Sinclair et al., 2018). Zn deficiency did not affect the mRNA levels of *MTP1* in mutants as compared to WT (Figure S9g). In WT, expression levels of *MTP3* were higher in roots than in shoots, whereas MTP3 expression in roots from mutant plants showed increased mRNA levels relative to WT irrespective of external Zn status (Figure S9h).

All mutants have altered seed development

We examined characteristics of seeds from WT and mutants to further elucidate the relationship between seed development and *ZIP* genes. When grown in soil, quadruple and triple mutants show no obvious visible phenotypes, as compared to WT (Figure S10a). Next, we dissected individual siliques and examined seeds from the quadruple and triple mutants to compare to WT at different developmental stages (Figure 4a). As compared to the young and green WT siliques, which had embryos of similar size and shape, siliques from quadruple and triple mutants exhibited several defects. Mutant siliques contained more aborted seeds, which appeared brown and shrunken (Figure 4a). Quantification of seed abortion revealed that 20.8, 17.2, and 16.6% of the seeds from *qko*, *tko-1*, and *tko-2* mutants aborted, respectively, while 3.2% of seeds were aborted in WT siliques (Figure 4b). The number of seeds per silique was also lower than that of WT (Figure 4c). At the late dry maturation stages, mutants contained aborted dark brown and small seeds, while WT mature siliques consisted of uniform brown seeds (Figure 4a). Seed length of mutants was also decreased (Figure 4d), and therefore the 100-seed mass of quadruple and triple mutants was significantly lower than WT (Figure 4e). We tested whether Zn supplementation could rescue the seed phenotypes of the mutants. WT and quadruple and triple mutants were grown side by side in soil and watered with 1 mM $ZnSO_4$ every week. Although Zn supplementation resulted in reduced growth compared to normal soil (Figure S10b), siliques from the WT and mutants were

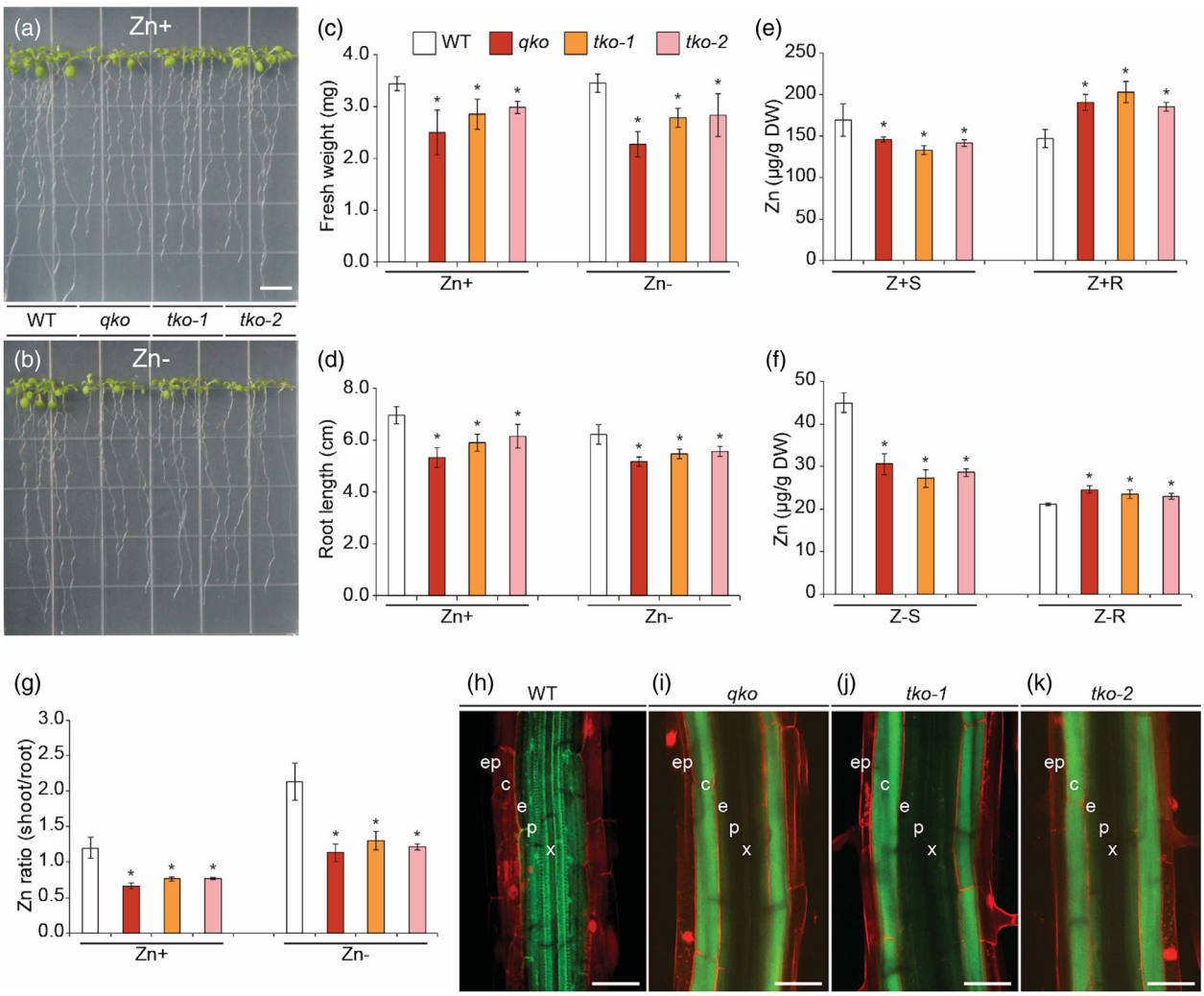

Figure 3. Seedling growth of triple and quadruple mutants. (a,b) Growth of wild type (WT) and mutant seedlings on Zn-sufficient (Zn+) (a) and Zn-deficient (Zn−) (b) medium. Photographs were taken 8 days after germination. Bars = 1 cm. (c,d) Fresh weight (c) and root length (d) of 15 seedlings of each line grown on Zn+ or Zn− medium. (e,f) Zn concentrations in shoots and roots from WT and quadruple and triple mutants grown under Zn+ (e) or Zn− (f) conditions for 8 days. Tissues were harvested, digested, and analyzed by inductively coupled plasma mass spectrometry (ICP-MS). (g) Zn shoot:root ratios of Zn concentrations were calculated from the data shown in panels (e) and (f). *qko, irt3-1/zip4-2/zip6-1/zip9-1*; *tko-1, irt3-1/zip4-2/zip6-1*; *tko-2, irt3-1/zip4-2/zip9-1*. Z+S, shoots from Zn-sufficient medium; Z+R, roots from Zn-sufficient medium; Z-S, shoots from Zn-deficient medium; Z-R, roots from Zn-deficient medium. Mean values and standard errors were obtained from four independent experiments. *$P < 0.05$ compared to WT. (h–k) Visualization of Zn localization in roots by Zinpyr-1. Confocal laser scanning microscopy images of roots of WT (h), *qko* (i), *tko-1* (j), and *tko-2* (k) stained with Zinpyr-1 and propidium iodide to visualize Zn (green) and cell walls (red). x, xylem; p, pericycle; e, endodermis; c, cortex; ep, epidermis. Bars = 50 μm.

indistinguishable, suggesting that the Zn supplement rescued the seed morphology of triple and quadruple mutants (Figure S10c).

We also analyzed the seed phenotype of the single and double mutant plants. When grown in soil, the seed number per silique of single and double mutants was similar to that of WT (Figure S11a). In contrast, the seed abortion rate of mutants was higher than that of WT (Figure S11b). Seed length was similar to that of WT (Figure S11c), while the 100-seed mass of mutants was significantly lower than WT (Figure S11d).

All mutants accumulate less metal ions in seeds

Because quadruple and triple mutants showed abnormal seed phenotypes, we next investigated metal accumulation and distribution in seeds. The Zn concentrations in seeds from the single and double mutant lines were significantly lower (83.3–91.2%) than that of WT (Figure S11e). Furthermore, the Zn concentrations of *qko*, *tko-1*, and *tko-2* mutants were 69.1, 72.5, and 69.2% compared to WT, respectively (Figure 5a). Interestingly, Fe, Cu, and Mn concentrations were also decreased in seeds from the single, double, triple, and quadruple mutants (Figure 5b–d;

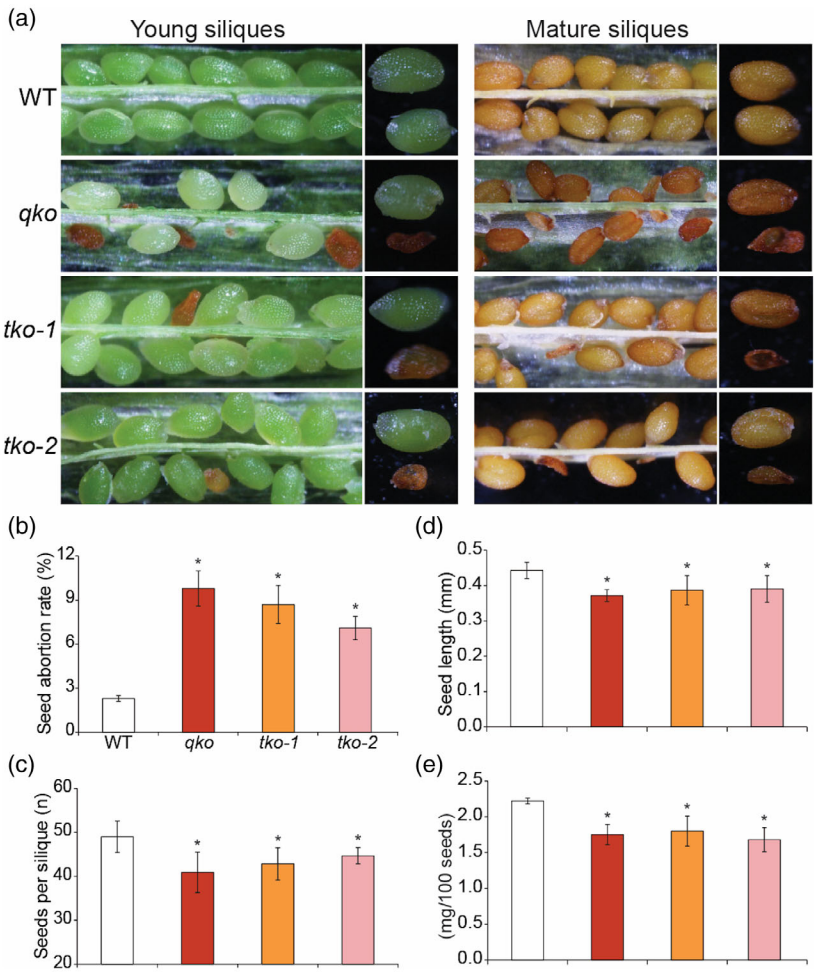

Figure 4. Altered seed development in triple and quadruple mutants. (a) Seed characteristics in the siliques from wild type (WT), the quadruple mutant, and two triple mutants. (b,c) Quantification of seed abortion in WT and mutants (b) and the number of seeds per silique (c). Values are mean ± standard error (SE) of 15–20 siliques from four independent plants. (d) Average seed length was measured after scanning the seeds via ImageJ software (https://imagej.nih.gov/ij/). Data are presented as mean ± SE of a minimum of 30 seeds. (e) Seed weight obtained by measuring 100 dry seeds ($n = 5$, mean ± SE). Asterisks above the bars indicate significant differences from WT (Student's *t*-test, $P < 0.05$).

Figure S11f–h). At present we cannot easily explain why the concentrations of these cations are also decreased in the mutants; as noted in a recent review by Kumar et al. (2021), more work is needed to understand how nutrient pathways interact and influence each other.

Next, we used synchrotron-based X-ray fluorescence (SXRF) elemental mapping to visualize the metal distribution in WT and quadruple and triple mutant seeds. High-resolution SXRF microtomography can be used to provide spatial localization and quantification of elements in plant tissues and has been successfully used to document unique localization patterns of micronutrients in seeds (Kim et al., 2006; Ricachenevsky et al., 2018). Zn was clearly less abundant in seeds from the quadruple mutant compared to WT, but there were no changes in distribution (Figure 5e). Two-dimensional imaging also showed less Zn in quadruple mutant seed, as compared to WT seeds (Figure S12a). Concentrations of other metals, such as Fe, Cu, and Mn also decreased as measured by inductively coupled plasma mass spectrometry (ICP-MS), but localization remained unchanged (Figure 5b–e). Seeds from triple mutants also had less Zn, consistent with ICP-MS analysis (Figure S12b).

DISCUSSION

Understanding the molecular basis of Zn uptake and transport in plants is critical for improving both the Zn content of plants and the ability of plants to grow in low-Zn soils. Our study demonstrates the importance of members of the ZIP family in root-to-shoot translocation of Zn as well as in proper seed development. Single or double mutants of *IRT3*, *ZIP4*, and *ZIP9*, three closely related *ZIP* genes, exhibited no apparent phenotypes as seedlings, whereas lines carrying mutations in all three of these *ZIP* genes had altered Zn distribution between shoots and roots, leading to impaired growth irrespective of external Zn status. This is a classic example of genetic redundancy where each of these three *ZIP* genes can compensate for loss of the other two genes. *zip6* single or double mutants also did not show any phenotypes as seedlings but the triple mutant of *irt3 zip4 zip6* had a very similar phenotype to that of the *irt3 zip4 zip9* triple mutant, showing altered distribution of

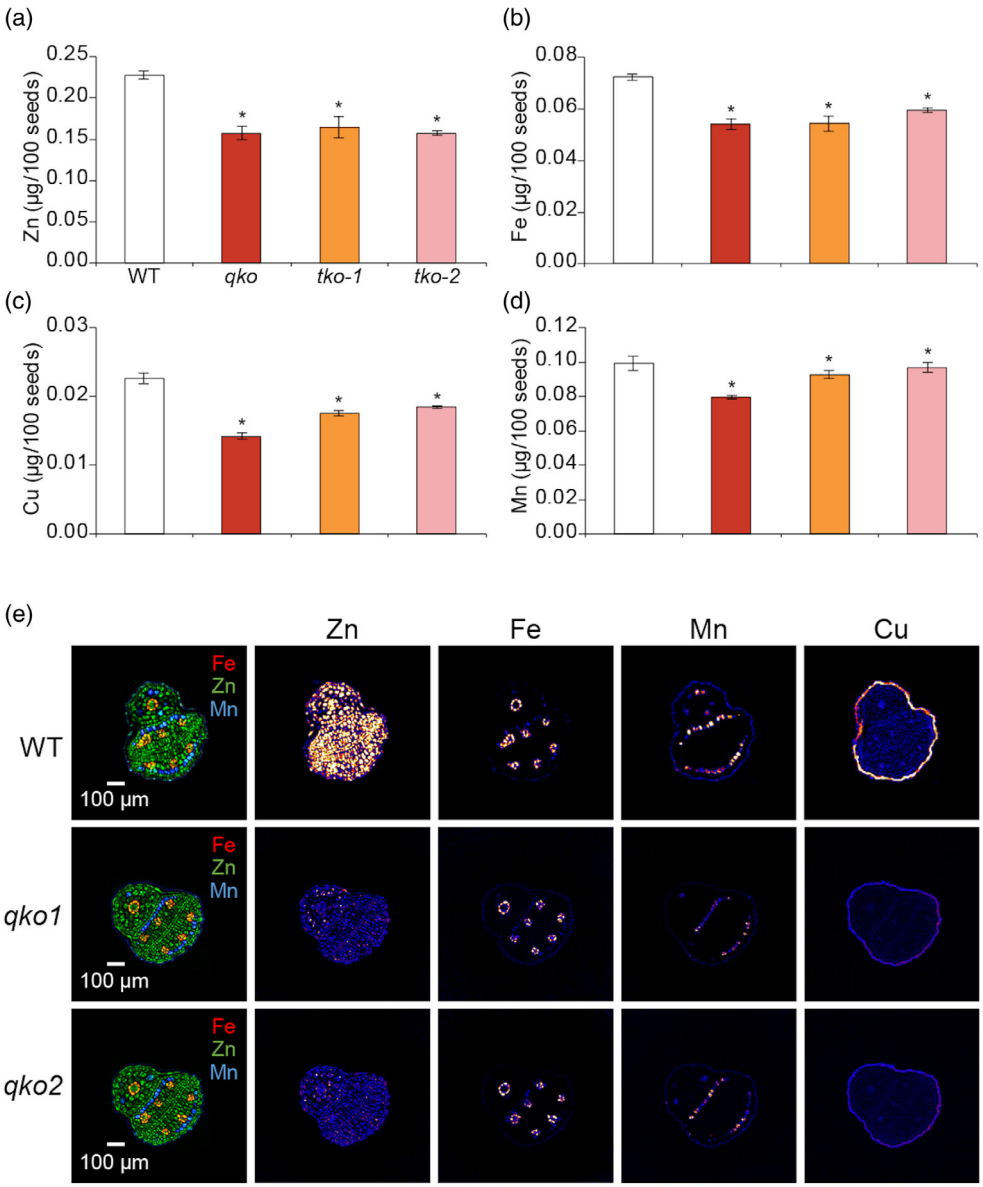

Figure 5. Metal content in mutant seeds measured by inductively coupled plasma mass spectrometry (ICP-MS) and synchrotron-based X-ray fluorescence (SXRF) tomograms of mutant seeds. (a–d) Quantification of Zn (a), Fe (b), Mn (c), and Cu (d) from WT, the quadruple mutant, and two triple mutants. Values are mean ± standard error (SE) of 100 seeds from four independent plants. Asterisks above the bars indicate significant differences between mutant lines and WT ($P < 0.05$). (e) SXRF microtomography of Arabidopsis seeds. (Left) SXRF composite images of Fe, Zn, and Mn internal distributions in WT (top) and *qko* (middle, bottom) seeds. (Right) Intensity-normalized SXRF tomographic slices of Zn Kα, Fe Kα, Mn Kα, and Cu Kα fluorescence for WT and *qko* seeds. Tomograms for each element are scaled to the highest maximum pixel abundance. On the color bar, cooler colors indicate lower abundance and warmer colors indicate higher abundance. *qko1* and *qko2* are two different seeds.

Zn between the root at the shoot. This suggests overlapping functions among these four genes and in the absence of ZIP6, ZIP9 can no longer compensate for the simultaneous loss of *IRT3* and *ZIP4*, even though *ZIP6* does not cluster phylogenetically with the other three *ZIP* genes. We propose that these four genes play a role in xylem loading based on the following considerations: (i) all are PM-localized Zn transporters; (ii) all four proteins are expressed in the central cylinder of the root; and (iii) Zn does not localize to the stele in the roots of triple and quadruple mutants. Our GUS expression data agree well with previously published IRT3-GUS data (Lin et al., 2009), ZIP4-GUS and ZIP4-GFP data (Lin et al., 2016), and ZIP6-GUS data (Spielmann et al., 2020). In addition, IRT3 has previously been shown to localize to the PM in agreement with our localization data.

The decreased ability to load Zn into the xylem then explains the lower levels of Zn observed in shoot tissues of the triple and quadruple mutants. This reduction of Zn translocation from root to shoot is similar to that reported for the *A. thaliana hma2 hma4* double mutant. In roots of the *hma2 hma4* double mutant, Zn was predominantly accumulated in the pericycle and endodermal cell layers, where *HMA2* and *HMA4* are normally expressed (Sinclair et al., 2007). Their lack of expression leads to a failure to export Zn into the xylem, whereas a lack of expression of *ZIP* genes leads to failure to load the xylem parenchyma cells with Zn. The net result is the same: less Zn for transport to the shoots.

Although single and double mutants showed seed phenotypes with higher seed abortion rates and decreased seed weight compared to WT, quadruple and triple mutants had more pronounced phenotypes, with fewer seeds per siliques, higher rates of seed abortion, and a reduction in seed weight compared to WT (Figure 4). Overall, the quadruple mutant had the most drastic seed phenotypes, likely owing to the additive effect of the disruption of four *ZIP* genes. The Zn concentration in the mature seed of all mutants was decreased relative to WT, but the quadruple mutant had the lowest seed Zn concentration, suggesting functional redundancy among these *ZIP* genes.

We can offer two possibilities for how disruption of *ZIP* genes leads to the observed seed phenotypes. One is that these four ZIP proteins directly affect seed development by loading Zn into seeds during the development of the endosperm and the embryo. The other is that the reduction in Zn translocation from root to shoot means that there is less Zn available to supply reproductive organs as they develop. And, of course, given that these *ZIP* genes are expressed in both the roots and developing seeds, it is most likely a combination of both. Such a dual role has been shown for HMA2 and HMA4 (Olsen et al., 2016). By grafting mutant shoots to WT roots to ensure that the HMA pumps were delivering Zn to the shoot, Olsen et al. (2016) could then see that the pumps were also needed in the developing seed.

In rice, two members of the ZIP family, OsZIP3 and OsZIP7, have been implicated in xylem loading and Zn distribution to developing grain. OsZIP7 is expressed in parenchyma cells of vascular bundles in roots and in nodes. It mediates Zn influx from the cortex to the pericycle in roots and is involved in intervascular transfer of Zn in nodes (Tan et al., 2019). OsZIP3 is localized to xylem transfer cells in enlarged vascular bundles (EVBs) of nodes and is involved in unloading of Zn from the xylem of EVBs (Sasaki et al., 2015).

The use of higher-order mutants has allowed us to show that four of the Zn-deficiency-inducible Zn transporters, IRT3, ZIP4, ZIP6, and ZIP9, in *A. thaliana* have overlapping functions. Future studies using cell-type-specific promoters to drive expression of the different *ZIP* genes may allow further dissection of how various ZIP family members contribute to Zn homeostasis.

EXPERIMENTAL PROCEDURES

Plant materials and growth conditions

Seeds were surface sterilized and plated on half-strength Murashige and Skoog (MS) medium supplemented with 0.5 g L^{-1} 2-(N-morpholino)ethanesulfonic acid, 1.5% sucrose, 0.8% agar, pH 5.8. Plates were kept at 4°C in the dark for 4 days before being incubated under constant light at 21°C for 7 days. Seedlings were then transferred to control, Zn-deficient, or Fe-deficient media. For Zn or Fe deficiency, the Zn chelator *N,N,N′,N′*-tetrakis (2-pyridinylmethyl)-1,2-ethanediamine (TPEN; 20 μM) was supplemented or the Fe chelator 3-(2-pyridyl)-5,6-diphenyl-1,2,4-triazine sulfonate (ferrozine; 300 μM) was added to the agar medium, respectively. The seedlings were grown for an additional 3 days and shoot and root samples from seedlings were frozen with liquid nitrogen for RNA isolation.

For the analysis of seedling phenotypes, sterilized seeds were sown on half-strength MS medium containing 15 μM $ZnSO_4$ (control; Zn-sufficient media), no added Zn (Zn−; Zn-deficient media) with 20 μM TPEN, or excess Zn (120 and 125 μM $ZnSO_4$). Plants were grown for 8 days. Both plate-grown and soil-grown plants were kept under 16/8-h light/dark conditions at 22°C.

Yeast growth conditions

Yeast cells were transformed with empty vector pDR195 or constructs containing ZIP cDNAs. Three yeast strains were used in these studies: the Zn uptake-defective mutant *zrt1/zrt2Δ* (*MATα ade6 can1 his3 leu2 trp1 ura3 zrt1*::LEU2 *zrt2*::HIS3), the Fe uptake-defective mutant *fet3/fet4Δ* (*MATa can1 his3 leu2 trp1 ura3 fet3*::HIS3 *fet4*::LEU2), and the Mn uptake-defective mutant *smf1Δ* (SLY8; *MATa ura3 lys2 ade2 trp1 his3 leu2 smf1*::HIS3). Yeast cells were transformed by the Li-acetate method (Gietz and Schiestl, 2007). Transformants were grown in an YPD medium (1% yeast extract, 2% peptone, and 2% glucose) and densities were adjusted to an OD_{600} of 1, 0.1, 0.01, or 0.001 by serial dilution. Afterward, 5-μl aliquots were spotted onto synthetic dropout agar medium supplemented with 20 g L^{-1} of glucose and the necessary auxotrophic supplements. Primers used to design expression constructs are listed in Table S1.

Quantitative reverse transcriptase-PCR

RNA was prepared from each tissue. cDNA was reverse transcribed from 1 μg RNA with M-MLV reverse transcriptase (New England Biolabs, Ipswich, MA, USA). qPCR analysis was performed to determine gene expression levels (ABI Model 7700; Thermo Fisher, Waltham, MA, USA) using a SYBR premix ExTaq kit (Takara Bio, Shiga, Japan). Primers used are listed in Table S1. Samples were run in triplicate and normalized to *EF1α*, and arbitrary transcriptional units were calculated. Values represent the average of three biological replicates.

Plasmid construction, histochemical GUS assay, and confocal microscopy analysis of GFP

For GUS constructs, promoter regions (approximately 1 kb) of *IRT3*, *ZIP4*, *ZIP6*, or *ZIP9* were amplified from WT genomic DNA with two specific primers (Table S1), and the fragment was subcloned into the pGEM T-easy plasmid (Promega, Madison, WI, USA) and sequenced. It was then excised by digestion and ligated

into pCAMBIA1381xA (CAMBIA). For the GFP constructs, the cDNAs spanning the entire open reading frame of *IRT3*, *ZIP4*, *ZIP6*, and *ZIP9* were amplified with two specific primers listed in Table S1. Amplicons were introduced into the pGEM T-easy plasmid (Promega) for sequencing. After digestion with *Nco*I and *Bgl*II, the fragments were inserted into pCAMBIA 1302 (CAMBIA). All constructs were moved into *Agrobacterium tumefaciens* strain GV3101 and transformants were used to transform plants using the floral dip method (Clough and Bent, 1998). Transformants were isolated by selection on agar medium containing hygromycin (25 mg ml^{-1}).

For GUS histochemical staining, plants were grown on half-strength MS medium with or without Zn for 4 days. Whole seedlings were incubated with the substrate 5-bromo-4-chloro-3-indolyl β-D-glucuronide as described (Jefferson et al., 1987). Laser scanning confocal microscopy (Leica TCS SP) was used to observe the GFP florescence from roots of transgenic plants stained with 10 mM PI.

Isolation of mutant lines

irt3-1 (WiscDsLox429D04) and *zip 6-2* (WiscDsLox233237_03O) were obtained from the *WiscDsLox* T-DNA collection (Woody et al., 2007). *zip4-2* (SALK_043236), *zip4-3* (SALK_145371), *zip6-1* (SALK_116013), and *zip9-1* (SALK_074682) were obtained from the SALK collection (Alonso et al., 2003). Homozygous lines were identified by PCR (Figure S4) using left border T-DNA-specific and gene-specific primers (Table S1). Double, triple, and quadruple mutant lines were obtained by crossing confirmed single mutants, and genotyping was performed on plants from the third generation after crossing.

Tissue elemental analysis

Samples were dried at 60°C for 3 days. Elemental analysis was done by ICP-MS as described (Lahner et al., 2003).

Zinpyr-1 staining

The Zn distribution in roots of WT and mutants was examined using Zinpyr-1, and PI was used to stain cell walls. Seven- to eight-days-old seedlings were washed three times in deionized water and immersed in a working solution of 20 μM Zinpyr-1 and incubated at room temperature in darkness for 3 h. Samples were rinsed in deionized water, immersed in 75 μM PI, and rinsed again. Preparation and staining of Zinpyr-1 and PI were performed as described previously (Sinclair et al., 2007). Images were obtained using a confocal microscope (LSM700; Carl Zeiss, Dublin, CA, USA) with excitation at 488 nm.

Synchrotron-based X-ray fluorescence computed microtomography

Internal distributions of Zn and other micronutrient elements in WT and mutant-line Arabidopsis seeds were measured *in vivo* by SXRF computed microtomography (F-CMT) using the X-ray fluorescence microprobe (XFM) beamline at the National Synchrotron Light Source II (NSLS-II) in Upton, NY. XFM beamline is designed for monochromatic operation (2.3–23 keV) and optimized for spatially resolved X-ray absorption spectroscopy in conjunction with element-specific imaging and microdiffraction. The XFM beamline can also be operated in a pink beam 'imaging' mode that delivers up to 1000× more flux than the XFM monochromatic beam. The XFM filtered pink beam (12–20 keV broadband) was focused by rhodium-coated, silicon Kirkpatrick–Baez mirrors to a 1-μm spot for F-CMT measurements of seeds. Seeds were mounted to a quartz post that was centered on a rotation stage attached to a fast-scanning translation stage. Seeds were translated horizontally through the focused X-ray beam in step sizes ranging from 2 to 4 μm and then rotated at intervals of between 0.5° and 1.5° angular steps, repeating the translation through a total of 360°. X-ray fluorescence spectra were recorded with a seven-element Canberra Mirion SXD-7 silicon drift detector coupled to Quantum Detectors Xspress3 electronics. Thin-film standard reference materials (SRM 1832 & 1833) were measured as part of the dataset to establish elemental sensitivities (counts per second μg cm^{-2}). Two-dimensional sinograms were computationally reconstructed using the filtered back projection method available in the LARCH package (Newville, 2013) to provide images of the cross-sectional internal element distribution.

Synchrotron-based X-ray imaging at the National Synchrotron Light Source and the Stanford Synchrotron Radiation Lightsource

Intact seeds were analyzed for metal distribution using SXRF at the now decommissioned beamline X26A of the National Synchrotron Light Source, Brookhaven National Laboratory as described in detail previously (Kim et al., 2006; Ricachenevsky et al., 2018) and at BL2-3 at the Stanford Synchrotron Radiation Lightsource as described previously (Ricachenevsky et al., 2021).

ACKNOWLEDGMENTS

This work was supported by U.S. Department of Energy (DOE) grant DE-FG02-06ER15809 to MLG, NSF grant DBI 0701119 to MLG and DES, NIH grant R01GM078536 to MLG and DES, and NIH grant P42ES007373 to MLG and TP. FKR was awarded a fellowship from CNPq (Conselho Nacional de Desenvolvimento Científico e Tecnológico). Use of the NSLS facility was supported by the Department of Energy under Contract DE-AC02-98CH10886. Use of the Stanford Synchrotron Radiation Lightsource, SLAC National Accelerator Laboratory, is supported by the U.S. Department of Energy, Office of Science, Office of Basic Energy Sciences under Contract No. DE-AC02-76SF00515. Parts of this research used the XFM Beamline of the National Synchrotron Light Source II, a DOE Office of Science User Facility operated for the DOE Office of Science by Brookhaven National Laboratory under Contract No. DE-SC0012704.

AUTHOR CONTRIBUTIONS

SL, JL, and MLG designed the research; SL, JL, FKR, TP, and RT performed the research; DES contributed new reagents/analytic tools; SL and MLG analyzed the data; SL, FKR, DES, and MLG wrote the paper.

CONFLICT OF INTEREST

The authors have declared no conflict of interest.

DATA AVAILABILITY STATEMENT

All relevant data can be found within the manuscript and its supporting materials.

SUPPORTING INFORMATION

Additional Supporting Information may be found in the online version of this article.

Figure S1. Complementation of yeast metal uptake mutants.

Figure S2. *In silico* expression analysis of *ZIP* genes during development.

Figure S3. ZIP-GFP translational fusion proteins localize to the plasma membrane.

Figure S4. T-DNA mutants.

Figure S5. Seedling phenotypes of single T-DNA mutants grown under Zn-sufficient or Zn-deficient conditions.

Figure S6. Seedling phenotypes of double mutants grown under Zn-sufficient or Zn-deficient conditions.

Figure S7. Measurement of Fe levels of WT and triple and quadruple mutants.

Figure S8. Increased Zn resistance of triple and quadruple mutants.

Figure S9. Quantitative RT-PCR analysis of Zn homeostasis-related genes at the seedling stage.

Figure S10. Growth morphology of WT and triple and quadruple mutants.

Figure S11. Characterization of seed phenotypes and metal contents in single and double mutants.

Figure S12. Synchrotron-based X-ray fluorescence (SXRF) elemental imaging of triple and quadruple mutants.

Table S1. List of primers used in this study.

REFERENCES

Alonso, J.M., Stepanova, A.N., Leisse, T.J., Kim, C.J., Chen, H., Shinn, P. *et al.* (2003) Genome-wide insertional mutagenesis of *Arabidopsis thaliana*. *Science*, **301**, 653–657.

Andreini, C., Bertini, I. & Rosato, A. (2009) Metalloproteomes: a bioinformatic approach. *Accounts of Chemical Research*, **42**, 1471–1479.

Arrivault, S., Senger, T. & Krämer, U. (2006) The Arabidopsis metal tolerance protein AtMTP3 maintains metal homeostasis by mediating Zn exclusion from the shoot under Fe deficiency and Zn oversupply. *The Plant Journal*, **46**, 861–879.

Cakmak, I. (2000) Possible roles of zinc in protecting plant cells from damage by reactive oxygen species. *New Phytologist*, **146**, 185–205.

Clough, S.J. & Bent, A.F. (1998) Floral dip: a simplified method for *Agrobacterium*-mediated transformation of *Arabidopsis thaliana*. *The Plant Journal*, **16**, 735–743.

Eide, D., Broderius, M., Fett, J. & Guerinot, M.L. (1996) A novel iron-regulated metal transporter from plants identified by functional expression in yeast. *Proceedings of the National Academy of Sciences of the United States of America*, **93**, 5624–5628.

Evens, N.P., Buchner, P., Williams, L.E. & Hawkesford, M.J. (2017) The role of ZIP transporters and group F bZIP transcription factors in the Zn-deficiency response of wheat (*Triticum aestivum*). *The Plant Journal*, **92**, 291–304.

Gietz, R.D. & Schiestl, R.H. (2007) Quick and easy yeast transformation using the LiAc/SS carrier DNA/PEG method. *Nature Protocols*, **2**, 35–37.

Grotz, N. & Guerinot, M.L. (2006) Molecular aspects of Cu, Fe and Zn homeostasis in plants. *Biochimica Et Biophysica Acta*, **1763**, 595–608.

Hu, J. (2021) Towards unzipping the ZIP transporters: structure, evolution and implications on drug discovery against cancer. *FEBS Journal*. https://doi.org/10.1111/febs.15658

Huang, S., Sasaki, A., Yamaji, N., Okada, H., Mitani-Ueno, N. & Ma, J.F. (2020) The ZIP transporter family member OsZIP9 contributes to root zinc uptake in rice under zinc-limited conditions. *Plant Physiology*, **183**, 1224–1234.

Hussain, D., Haydon, M.J., Wang, Y., Wong, E., Sherson, S.M., Young, J. *et al.* (2004) P-type ATPase heavy metal transporters with roles in essential zinc homeostasis in Arabidopsis. *The Plant Cell*, **16**, 1327–1339.

Inaba, S., Kurata, R., Kobayashi, M., Yamagishi, Y., Mori, I., Ogata, Y. *et al.* (2015) Identification of putative target genes of bZIP19, a transcription factor essential for Arabidopsis adaptation to Zn deficiency in roots. *The Plant Journal*, **84**, 323–334.

Jefferson, R.A., Kavanagh, T.A. & Bevan, M.W. (1987) GUS fusions: beta-glucuronidase as a sensitive and versatile gene fusion marker in higher plants. *EMBO Journal*, **6**, 3901–3907.

Kawachi, M., Kobae, Y., Mori, H., Tomioka, R., Lee, Y. & Maeshima, M. (2009) A mutant strain *Arabidopsis thaliana* that lacks vacuolar membrane zinc transporter MTP1 revealed the latent tolerance to excessive zinc. *Plant and Cell Physiology*, **50**, 1156–1170.

Kim, S.A., Punshon, T., Lanzirotti, A., Li, L., Alonso, J.M., Ecker, J.R. *et al.* (2006) Localization of iron in *Arabidopsis* seed requires the vacuolar membrane transporter VIT1. *Science*, **314**, 1295–1298.

Krämer, U. & Clemens, S. (2005) Functions and homeostasis of zinc, copper and nickel in plants. In: Tamás, M. & Martinoia, E. (Eds.) *Topics in current genetics 14*. Heidelberg, Germany: Springer, pp. 215–271.

Kumar, S., Kumar, S. & Mohapatra, T. (2021) Interaction between macro- and micro-nutrients in plants. *Frontiers in Plant Science*, **12**, https://doi.org/10.3389/fpls.2021.665583

Lahner, B., Gong, J., Mahmoudian, M., Smith, E.L., Abid, K.B., Rogers, E.E. *et al.* (2003) Genomic scale profiling of nutrient and trace elements in *Arabidopsis thaliana*. *Nature Biotechnology*, **21**, 1215–1221.

Lilay, G.H., Persson, D.P., Castro, P.H., Liao, F., Alexander, R.D., Aarts, M.G.M. *et al.* (2021) *Arabidopsis* bZIP19 and bZIP23 act as zinc sensors to control plant zinc status. *Nature Plants*, **7**, 137–143.

Lin, Y.F., Hassan, Z., Talukdar, S., Schat, H. & Aarts, M.G. (2016) Expression of the ZNT1 Zinc transporter from the metal hyperaccumulator *Noccaea caerulescens* confers enhanced zinc and cadmium tolerance and accumulation to *Arabidopsis thaliana*. *PLoS One*, **11**, e0149750.

Lin, Y.F., Liang, H.M., Yang, S.Y., Boch, A., Clemens, S., Chen, C.C. *et al.* (2009) Arabidopsis IRT3 is a zinc-regulated and plasma membrane localized zinc/iron transporter. *New Phytologist*, **182**, 392–404.

Milner, M.J., Seamon, J., Craft, E. & Kochian, L.V. (2013) Transport properties of members of the ZIP family in plants and their role in Zn and Mn homeostasis. *Journal of Experimental Botany*, **64**, 369–381.

Newville, M. (2013) Larch: an analysis package for XAFS and related spectroscopies. *Journal of Physics: Conference Series*, **430**, 012007.

Olsen, L.I., Hansen, T.H., Larue, C., Østerberg, J.T., Hoffmann, R.D., Liesche, J. *et al.* (2016) Mother-plant-mediated pumping of zinc into the developing seed. *Nature Plants*, **2**, 16036.

Palmer, C.M. & Guerinot, M.L. (2009) A question of balance: facing the challenges of Cu, Fe and Zn homeostasis. *Nature Chemical Biology*, **5**, 333–340.

Palmgren, M.G., Clemens, S., Williams, L.E., Krämer, U., Borg, S., Schjørring, J.K. *et al.* (2008) Zinc biofortification of cereals: problems and solutions. *Trends in Plant Science*, **13**, 464–473.

Ricachenevsky, F.K., Punshon, T., Lee, S., Oliveira, B., Trenz, T.S., Maraschin, F. *et al.* (2018) Elemental profiling of rice FOX lines leads to characterization of a new Zn plasma membrane transporter, OsZIP7. *Frontiers in Plant Science*, **9**, 865.

Ricachenevsky, F.K., Punshon, T., Salt, D.E., Fett, J.P. & Guerinot, M.L. (2021) *Arabidopsis thaliana* zinc accumulation in leaf trichomes is correlated with zinc concentration in leaves. *Scientific Reports*, **11**, 5278.

Sasaki, A., Yamaji, N., Mitani-Ueno, N., Kashino, M. & Ma, J.F. (2015) A node-localized transporter OsZIP3 is responsible for the preferential distribution of Zn to developing tissues in rice. *The Plant Journal*, **84**, 374–384.

Schuler, M., Rellán-Álvarez, R., Fink-Straube, C., Abadía, J. & Bauer, P. (2012) Nicotianamine functions in the phloem-based transport of iron to sink organs, in pollen development and pollen tube growth in *Arabidopsis*. *The Plant Cell*, **24**, 2380–2400.

Sinclair, S.A. & Krämer, U. (2012) The zinc homeostasis network of land plants. *Biochimica Et Biophysica Acta*, **1823**, 1553–1567.

Sinclair, S.A., Senger, T., Talke, I.N., Cobbett, C.S., Haydon, M.J. & Krämer, U. (2018) Systemic upregulation of MTP2- and HMA2-mediated Zn partitioning to the shoot supplements local Zn deficiency responses. *The Plant Cell*, **30**, 2463–2479.

Sinclair, S.A., Sherson, S.M., Jarvis, R., Camakaris, J. & Cobbett, C.S. (2007) The use of the zinc-fluorophore, Zinpyr-1, in the study of zinc homeostasis in *Arabidopsis* roots. *New Phytologist*, **174**, 39–45.

Spielmann, J., Ahmadi, H., Scheepers, M., Weber, M., Nitsche, S., Carnol, M. *et al.* (2020) The two copies of the zinc and cadmium ZIP6 transporter of *Arabidopsis halleri* have distinct effects on cadmium tolerance. *Plant, Cell and Environment*, **43**, 2143–2157.

Tan, L., Qu, M., Zhu, Y., Peng, C., Wang, J., Gao, D. *et al.* (2020) ZINC TRANSPORTER5 and ZINC TRANSPORTER9 function synergistically in zinc/cadmium uptake. *Plant Physiology*, **183**, 1235–1249.

Tan, L., Zhu, Y., Fan, T., Peng, C., Wang, J., Sun, L. *et al.* (2019) OsZIP7 functions in xylem loading in roots and inter-vascular transfer in nodes to

deliver Zn/Cd to grain in rice. *Biochemical and Biophysical Research Communications*, **512**, 112–118.

Woody, S.T., Austin-Phillips, S., Amasino, R.M. & Krysan, P.J. (2007) The *WiscDsLox* T-DNA collection: an Arabidopsis community resource generated by using an improved high-throughput T-DNA sequencing pipeline. *Journal of Plant Research*, **120**, 157–165.

Wu, J., Zhao, F.J., Ghandilyan, A., Logoteta, B., Guzman, M.O., Schat, H. *et al.* (2009) Identification and functional analysis of two ZIP metal transporters of the hyperaccumulator *Thlaspi caerulescens*. *Plant and Soil*, **325**, 79–95.

Yang, M., Li, Y., Liu, Z., Tian, J., Liang, L., Qiu, Y. *et al.* (2020) A high activity zinc transporter OsZIP9 mediates zinc uptake in rice. *The Plant Journal*, **103**, 1695–1709.